Work-Amplitude Optimal Actuation of Nonlinear Resonant System

Mohammad Kurdi,[*] Philip Beran,[†] and Richard Snyder[‡]

Air Force Research Laboratory, WPAFB OH 45433.

In this study, we examine a new approach for actuation of dynamical systems with minimum work while maintaining constraints on system response and actuation force. Recently, we applied the approach to a lightly damped, linear oscillator. Here, we extend the method to nonlinear, resonant systems. Two methodology issues are addressed in the paper: sensitivity analysis about the nonlinear transient response and exploration of the strongly nonlinear relationship between the objective function and the actuation design variables. The optimization analysis is carried out on a lightly damped Duffing system of hardening and softening nonlinearities.

With a hardening nonlinear spring, the optimization formulation is assessed for dependence of nonlinear response on initial conditions. The formulation of the two-objective problem is found ideally suited to resolve the difficulty of dependence of response on initial conditions. The tradeoff curve of minimum work and maximum amplitude is computed. In comparison to harmonic actuation, the optimal actuation is found to yield the target amplitude with 2.2% savings in expended work and 17% reduction in the force amplitude. In some other designs, work savings amount to 135%. The optimal actuation strove to compensate for the limited force amplitude by an abrupt change in the force in time. With a spring with both softening and hardening, similar work savings and robustness of the optimization were demonstrated. In addition, the optimization search taps into regions of the response deemed discontinuous using harmonic actuation.

I.   Introduction

The design of an actuation force providing minimum-work performance is motivated by increasing interest in micro air vehicles (MAVs), where it is desired to operate the vehicle with the least amount of actuation work or actuation force for a desired displacement amplitude.[1–4] The MAVs are designed to favor resonant response characteristics in an effort to minimize their power expenditure.[5] Driving these systems to their optimal performance may trigger nonlinear response of the system. This work develops an effective optimization methodology to compute the optimal actuation of nonlinear resonant systems for minimum work and maximum amplitude considering limited force amplitude.

In a previous study, the work and amplitude optimal actuation force was computed for a linear dynamic system using a gradient-based optimization approach.[6,7] For a limited force amplitude the optimal design provided a 25% increase in the displacement amplitude over that possible using a harmonic excitation. The optimal actuation force was found to favor a snap-type variation (similar to that exhibited in biomechanical actuated systems[8]). Additionally, the optimal actuation frequency approached the natural frequency of the system (although not exactly equal) as the demand for larger displacement amplitude increased, but favored lower frequencies at lower amplitudes.

A challenging aspect in the design of dynamic systems is the need to evaluate the system response over an entire time interval in order to satisfy the constraints and evaluate the objective function. Different methods exist to enforce the constraints over the time interval. The constraints may be enforced at the global extremum,[9] at closely spaced points,[10] or more efficiently at only the local extrema of the response.[11–13] In

---

[*]NRC Research Associate, AFRL/RBSD, 2210 8th Street, Bldg 146, WPAFB, OH 45433. mhkurdi@gmail.com.

[†]Principal Research Aerospace Engineer, AFRL/RBSD. AIAA Associate Fellow. Philip.Beran@wpafb.af.mil.

[‡]Research Engineer, AFRL/RBSD. Richard.Snyder@wpafb.af.mil.

American Institute of Aeronautics and Astronautics

this study, since we are interested in maximizing the amplitude of the response, the amplitude constraint is enforced at only the global maximum, where a one-dimensional optimization search is used to locate the maximum.

Only the time-periodic characteristics of the work-and-amplitude performance measures are considered, since transient behavior of the system is soon damped out. The time-periodic response of the nonlinear system is computed using the spectral element method in time over one cycle. The spectral element method[14] combines the local flexibility of the finite element method with high-order Lagrange polynomials interpolated at time grid points corresponding to Gauss-Lobatto-Legendre polynomials. A monolithic-time approach is favored here so as to transform the nonlinear time-dependent differential equation into an explicit algebraic form. This allows a more direct computation of the response sensitivity.

The actuation force is parameterized using many design variables and represented using cubic splines. A gradient-based optimization approach is used to find the optimal actuation force, where an adjoint sensitivity analysis is developed to compute sensitivities of the performance measures with respect to the design variables. The computational cost of computing the sensitivity using the adjoint method is independent of the number of design variables. This enables an efficient optimization search due to the large number of design variables required to simulate the actuation.

In this paper, we consider the optimal actuation force of nonlinear dynamic systems that exhibit resonant behaviors. The formulation is applied to a forced Duffing oscillator[15, 16] with softening and hardening spring nonlinearities. The two-objective problem of minimum work and maximum amplitude is formulated using the constraint method, where the minimum-work force is computed for a set of target displacement amplitudes. A tradeoff curve of the two objectives is computed, where an improvement in one objective results in a deterioration in the second objective.[17] The inherent dependence of nonlinear response on initial conditions is resolved by the optimization formulation. Results of the optimization search are compared to trivial designs, where the optimal actuation force is found to favor snap-type variation over a harmonic force with large amplitude.

The paper proceeds with the formulation of the dynamic optimization problem in Section II. The computation of the time-periodic response using the spectral element method is described in Section III. The adjoint sensitivity of the nonlinear response is presented in Section IV. Finally the optimization methodology is applied to the Duffing system in Section V.

II.   Formulation of Work-Optimal Optimization Problem

The optimization problem is to find the periodic actuation force which minimizes the amount of actuation work over a cycle W for a specified target of displacement amplitude Γ_{T_i}:[6]

$$\min_{b} \quad W \tag{1a}$$

subject to

$$\max(|x_{ca}|) \geq \Gamma_{T_i} \qquad i = 1, ..., N, \tag{1b}$$

where b is the vector of design variables, which consist of the magnitudes of the actuation force f at equally spaced locations in one cycle (see Figure 1), and the circular forcing frequency, ω. The time-periodic response in the direction of actuation force f is denoted by x_{ca}. The subscripts c and a refer to the cyclic response and degree-of-freedom in direction of actuation, respectively. The index N refer to the total number of times the optimization problem is solved. The force design variables (6 variables in Figure 1) are allowed to change in the interval $[-f_{\max}, f_{\max}]$ during the optimization search. The period T of the response cycle is equal to the forcing period $T = 2\pi/\omega$. The time interval t is scaled by T leading to a scaled cycle s of length 1. The work expended during one scaled cycle (referred to as work henceforth), W, is

$$W = \int_0^1 f(s)\dot{x}_{ca}ds. \tag{2}$$

The $\dot{}$ symbol refer to derivative with respect to s. To evaluate the work and enforce the amplitude constraint (1b), the time-periodic response is computed using the spectral element (SE) method in a monolithic-time approach. In contrast to time-stepping methods, where the solution is unavailable between two time steps, the SE method computes the time-dependent solution over the whole cycle.

American Institute of Aeronautics and Astronautics

Once a SE solution of sufficient accuracy is constructed, the extrema are located by implementing a one dimensional optimization search. The target constraint is then enforced on the global extremum.[12, 13] Note that the location of the critical time points may drift as b is iterated. Therefore, the extrema locations are recomputed during the design process.

The integral in (2) is computed using Gauss-Lobatto-Legendre quadrature [18, page 56], where cubic splines are used to interpolate the actuation force to the Gauss-Lobatto-Legendre grid point. During design iterations the force design variables may change abruptly. In order to maintain an accurate interpolation using the cubic splines, the number of design points must be chosen less than the number of degrees of freedom in the SE method.[7]

The optimization problem is then solved one time for each target displacement for a total number of N times to construct the tradeoff curve of minimum work per cycle and maximum displacement amplitude. For each design on the tradeoff curve, the optimal actuation force (Figure 1) and frequency are computed. The tradeoff curve, although expensive to compute, provides the designer with all possible optimal designs of the two objectives, thereby allowing selection of the best design fitting user criteria.

Alternatively, the optimization problem of minimum work and maximum amplitude under limited force may be formulated by maximizing the response amplitude for a set of constraints on the work objective. Although this should lead to similar results to that of (1) the latter formulation is more effective for the design of nonlinear systems due to dependence on initial conditions (more on this in Section 1).
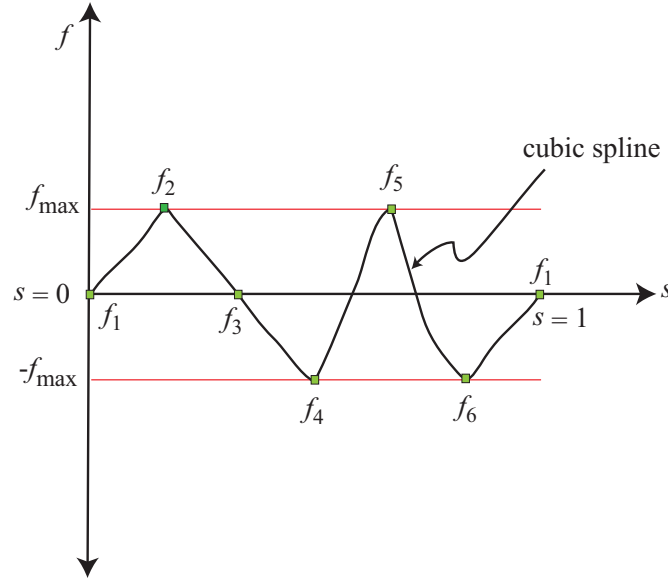

Figure 1. Schematic of the actuation force modeled using 6 force design variables in a cycle. The force value between two design variables is computed using cubic splines.

III.   Temporal Spectral Element Method

The spectral element (SE) method in time is applied to a set of first-order differential equations. Higher order unsteady terms can easily be tackled by transforming to first-order form. The coupled set of differential equations is,

$$\frac{\mathrm{d}x}{\mathrm{d}t} + \mathbf{A_s}x = f(x,t), \tag{3}$$

where x represents the collocated dependent variables $x \in R^{N_v}$, N_v is the number of dependent variables, time t is the independent variable, and $f(x,t)$ is a nonlinear function of x and t. The equations are coupled through the matrix $\mathbf{A_s}$, which is assumed to be time invariant.

For transient analysis of (3) initial conditions need to be enforced. However, this is generally not the case when cyclic solutions of (3) are sought, i.e., those that are time-periodic in response to a linear time-periodic

American Institute of Aeronautics and Astronautics

forcing function, $f(x,t) = f(x, t + T)$ of period T. For nonlinear time-periodic f the initial conditions are still not enforced. However, dependence of nonlinear response on initial conditions is achieved by specifying different initial guess of solution.

In this paper, our focus is on time-periodic responses. However, we present the SE method for both transient and cyclic analysis for completeness.

1st element   last element, N_{el}
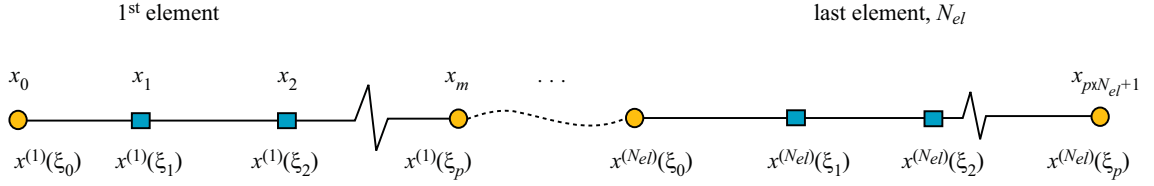
Figure 2. Discretization of the time domain into N_{el} elements represented by an p order Lagrange polynomial within each element. Nodes of each element are placed at zeros of Lobatto polynomials.

A.   Transient Analysis

The transient behavior (history) of each dependent variable can be discretized using spectral elements,[18] where the approximate p^{th}-order solution in each element is:

$$\hat{x}^{(j)}(\zeta) = \sum_{k=0}^{p} x^{(j)}(\zeta_k)\psi_k^{(j)}(\zeta). \tag{4}$$

Here $\psi_k^{(j)}$ represents the Lagrange polynomial of order k in element j, ζ_k are the zeros of the Lobatto-Legendre polynomials defined on the interval $\zeta \in [-1, 1]$ and $x^{(j)}(\zeta_k)$ are the unknown nodal values placed at ζ_k for element j. See Fig. (2), where the physical time domain $t \in [t_j, t_{j+1}]$ is transformed to the ζ domain for each element. The Lobatto polynomials L_{o_i} are a set of orthogonal polynomials that can be defined as the derivatives of order $i + 1$ Legendre polynomials,[19] L_i:

$$L_{o_i}(\zeta) \equiv L'_{i+1}(\zeta), \tag{5}$$

where the Legendre polynomials are defined explicitly as

$$L_i(\zeta) = \frac{1}{2^i i!} \frac{\mathrm{d}^i(\zeta^2 - 1)^i}{\mathrm{d}\zeta^i}. \tag{6}$$

The SE solution is obtained by: 1) substituting the trial solution $\hat{x}^{(j)}$ into the differential equation (3); 2) minimizing the residual in each element using the Bubnov-Galerkin method;[20] and 3) assembling the N_{el} time elements after enforcing inter-element continuity (more details can be found in 21). For one dependent variable matrix $\mathbf{A_s}$ becomes a scalar A_s and the discretized form of the differential equation reduces to

$$\mathbf{L}_c X_c = A_s \mathbf{L}_\omega X_c - \mathbf{L}_\omega F(X_c), \tag{7}$$

where $\mathbf{L}_c$ and $\mathbf{L}_\omega$ are the global differentiation and weight matrices, F is the global weighted form of the excitation and

$$X_c = \begin{bmatrix} x\big|_{t_0} & x\big|_{t_1} & \cdots & x\big|_{t_{p \times N_{el}+1}} \end{bmatrix}^T \tag{8}$$

is the SE solution of the dependent variable x collocated at all nodal times (redundant shared elements nodes are removed using inter-element continuity). The initial condition is applied by replacing the first row and column of $\mathbf{L}_c$ with zeros except for the first element, which is replaced with one. Also, the first element in $\mathbf{L}_\omega$ is replaced with zero and the first element in $-\mathbf{L}_\omega F$ is replaced with the value of x at $t = 0$. The SE solution X_c in (7) can then be computed using iterative methods. However, for a strictly time-dependent forcing function (not function of X_c) both direct and iterative methods can be used. See Section C.

B.   Cyclic Analysis

In some problems, such as damped systems with periodic forcing functions or self-excited nonlinear systems exhibiting limit cycle oscillations (LCO), the interest lies in the time-periodic response of the system, where $T = 2\pi/\omega$ is the period of the dynamic response. In this case, it is computationally advantageous to compute the steady-state cycle without simulating the transients.

For time-periodic or cyclic responses, the time cycle is discretized spectrally in the same way as in the transient solution. However, assembly of global matrices $\mathbf{L}_c$ and $\mathbf{L}_\omega$ is different. Here, the initial conditions are not imposed. Periodicity of the array of elements is enforced by requiring that the end node in the last element to be the initial node of the first element:

$$x^{(1)}(\zeta_0) = x^{(N_{el})}(\zeta_p). \tag{9}$$

Contributions to the end node in the last element are added to contributions from first element. Consequently, the last row and column of $\mathbf{L}_c$ are added to their counterpart in the first row and column. Therefore, the solution vector, X_c, becomes

$$X_c = \begin{bmatrix} x\big|_{t_0} & x\big|_{t_1} & \cdots & x\big|_{t_{p \times N_{el}}} \end{bmatrix}^T. \tag{10}$$

C.   Global Assembly and Solution

A number of dependent variables, N_v, can be handled through spatial connectivity matrix $\mathbf{A}_s$ of size $N_v \times N_v$ (boldface capital symbols are used to denote matrices). Here, the tensor product is introduced in (7) to give the global form of the system for N_v dependent variables:

$$\mathbf{L}_{cg} X_{cg} = \mathbf{A}_{cg} X_{cg} - \mathbf{L}_{\omega g} F_{cg}(X_{cg}), \tag{11}$$

where $\mathbf{L}_{cg}$ is the tensor product of the identity matrix (of size $N_v \times N_v$) and $\mathbf{L}_c$. In a similar fashion, the $\mathbf{A}_{cg}$ and $L_{\omega g}$ matrices are constructed. The vector X_{cg} is a collocation of all dependent variables at nodal times grouped by their corresponding dependent variables, N_v. For a transient solution, X_{cg} takes the form:

$$X_{cg} = \left[\left\{ \begin{array}{c} x_1\big|_{t_0} \\ x_1\big|_{t_1} \\ \vdots \\ x_1\big|_{t_{p \times N_{el}+1}} \end{array} \right\}^T \quad \cdots \quad \left\{ \begin{array}{c} x_{N_v}\big|_{t_0} \\ x_{N_v}\big|_{t_1} \\ \vdots \\ x_{N_v}\big|_{t_{p \times N_{el}+1}} \end{array} \right\}^T \right]^T. \tag{12}$$

A compact form of (11) becomes

$$\mathbf{Q} X_{cg} = -\mathbf{L}_{\omega g} F_{cg}(X_{cg}), \tag{13}$$

where

$$\mathbf{Q} \equiv \mathbf{L}_{cg} - \mathbf{A}_{cg}. \tag{14}$$

Equation (13) can be solved using Newton's method. By identifying a residual R we can evaluate the degree to which (13) is satisfied:

$$R(X_{cg}) \equiv \mathbf{Q} X_{cg} + \mathbf{L}_{\omega g} F_{cg}(X_{cg}). \tag{15}$$

A first-order Taylor series expansion of the nonlinear formula (15) gives

$$R^{\nu+1} = R^\nu + \mathbf{J} \Delta X_{cg}, \tag{16}$$

where

$$\mathbf{J} = \mathbf{Q} + \mathbf{L}_{\omega g} \frac{\partial F_{cg}}{\partial X_{cg}}. \tag{17}$$

The correction to a current approximation X_{cg} is computed by setting the residual, $R^{\nu+1}$ in (16) to zero. To facilitate convergence, we apply a relaxation parameter λ to the correction:

$$X_{cg}^{\nu+1} = X_{cg}^\nu + \lambda \Delta X_{cg}. \tag{18}$$

Note that when the forcing function is linear (independent of X_{cg}), the last term in (17) and updated residual in (16) are zero. Then for $\lambda = 1$, the solution X_{cg} can be evaluated from (18) in one iteration.

American Institute of Aeronautics and Astronautics

IV. Adjoint Sensitivity

In the optimization problem (1), the control force is represented using a large number of design variables. To carry out a gradient-based optimization search, the sensitivities of the objective and constraints need to be evaluated. The adjoint method[7] is used here to compute the gradients. The method is attractive due to the independence of the computational cost from the number of design variables. The gradient of the objective function W (2) is

$$\frac{\partial W}{\partial b} = \int_0^1 \left[\frac{\partial f_g}{\partial b}^T X_{cg} + f_g^T \frac{\partial X_{cg}}{\partial b} \right] ds, \tag{19}$$

where f_g is the cubic-spline interpolated value of the actuation force at a Gauss-Lobatto-Legendre grid point. With the finite-difference approach, the computational cost of computing this gradient is proportional to the product of the cost of computing the response X_{cg}, with the number of design variables. To eliminate the cost of recomputing X_{cg} when calculating the sensitivity to a design variable change, we compute $\frac{\partial X_{cg}}{\partial b}$ by defining the performance function h:

$$h(b) = X_{cg}. \tag{20}$$

The adjoint matrix is derived by adding the sensitivity of h to a change in b to the product of the adjoint matrix and the sensitivity of the response in (13):

$$\frac{\mathrm{d}h}{\mathrm{d}b} = \frac{\mathrm{d}X_{cg}}{\mathrm{d}b} + \mathbf{\Lambda}\mathbf{Q}\frac{\mathrm{d}X_{cg}}{\mathrm{d}b} + \mathbf{\Lambda}\left(\mathbf{L}_{\omega g}\frac{\partial F_{cg}}{\partial b} + \frac{\mathrm{d}\mathbf{Q}}{\mathrm{d}b}X_{cg} \right). \tag{21}$$

The adjoint matrix becomes the solution to

$$\mathbf{I} = -\mathbf{\Lambda}\mathbf{Q}, \tag{22}$$

where $\mathbf{I}$ is the identity matrix. After evaluating the adjoint matrix, $\mathbf{\Lambda}$ (21) is reduced to

$$\frac{\mathrm{d}h}{\mathrm{d}b} = \mathbf{\Lambda}\left(\mathbf{L}_{\omega g}\frac{\partial F_{cg}}{\partial b} + \frac{\mathrm{d}\mathbf{Q}}{\mathrm{d}b}X_{cg} \right). \tag{23}$$

The sensitivity of X_{cg} is now computed by evaluating $\mathbf{\Lambda}$ from (22) and substituting into (23) without the need to recompute the response X_{cg}. Additionally, the gradient of the objective W can then evaluated by inserting (23) into (19).

V. Forced Duffing Oscillator

The forced Duffing oscillator models the dynamic response of damped elastic structures with large non-linear displacements. Typically, the Duffing system consists of a cubic restoring force [22, page 158]. In this work, a pentic restoring force is additionally considered:

$$\ddot{x} + 2\zeta\omega_n\dot{x} + \omega_n^2(x + \beta x^3 + \gamma x^5) = \frac{a}{m}f(t), \tag{24}$$

where ζ is the damping factor, ω_n is the linear natural circular frequency, β is the coefficient of cubic nonlinearity, γ is the coefficient of pentic nonlinearity, m is the mass of the system, and $f(t) = f(t + T)$ is the periodic actuation with an amplitude of a. Depending on the sign of the coefficients β and γ, the stiffness of the system may increase or decrease nonlinearly. A positive or negative sign results in a hardening or softening nonlinearity, respectively.

Below we consider the dependence of cyclic solutions on initial conditions, and asses the convergence properties of the solution method (see Appendix A). We also apply the optimization to a hardening and to a hardening-and-softening springs to establish the benefits of the optimal actuation.

A. Analysis

The SE method in time is applied to compute the time-periodic response of the Duffing system. Equation (24) is cast in cyclic form

$$\frac{1}{T^2}\ddot{x}_{ca} + \frac{2}{T}\zeta\omega_n\dot{x}_{ca} + \omega_n^2(x + \beta x_{ca}^3 + \gamma x_{ca}^5) = \frac{a}{m}f(s) \tag{25}$$

by normalizing the time t with the forcing period T and introducing a scaled time: $s = t/T$. The single and double dots in (25) now mean $\frac{\mathrm{d}}{\mathrm{d}s}$ and $\frac{\mathrm{d}^2}{\mathrm{d}s^2}$, respectively. The solution is computed after transforming the second-order differential equation into first-order by introducing the variables $x_1 = x_{ca}$ and $x_2 = \dot{x}_{ca}$. The solution of (25) is computed for the parameters listed in Table 1, which correspond to a strictly cubic hardening case analyzed by Lee et al.[23]

<div align="center">

Table 1. Duffing equation parameters analyzed in Section A.

ω_n	ζ	m	a	$f(t)$	β	γ
1	0.05	1	0.4	$\sin \omega t$	0.1	0

</div>

The response is computed using the cyclic SE method. The accuracy of the SE solution depends on the number of elements and Lagrange polynomial order. For a smoothly varying function the SE solution of 25 DOF ($N_{el} = 5$ and $p = 5$) gives high accuracy.[21] Here we use a conservative number of DOFs ($N_{el} = 10$ and $p = 5$) in anticipation of sharp variation in the response. The displacement amplitude is reported in Figure 3a as a function of the circular actuation frequency ω: $\omega T = 2\pi$. To the right of natural frequency $\omega_n = 1$, the frequency response indicates two solutions in the region of $\omega = [1.2 - 1.3]$. In "this" fine region, the equilibrium solution of the cyclic analysis depends on the initial guess in the Newton method. The cyclic SE solution converges to one closer to the initial guess. For example, the upper branch cyclic solution results from an initial guess amplitude of $x_1 = 4$, whereas the lower branch solution results from an initial guess closer to the lower one. The cyclic solutions corresponding to these initial guesses are reported in Figures 3b and 3c, respectively. The initial guess is additionally noted in the figures. Note that in transient analysis, the initial guess corresponds to the set of initial conditions. An initial condition close to the upper branch (for example $x(0) = 4$ and $\dot{x}(0) = 0$) converges to a steady state solution at that branch.[23] This behavior can be used to our advantage in implementing the optimization search by capitalizing on dependence of the response on the initial guess.

The optimization search (discussed next) is implemented using a gradient-based optimization method in which the provided gradients guide the search. The adjoint method allows an efficient and accurate computation of the gradients. Consider, for example, the two cyclic solutions around $\omega = 1.2$. The adjoint sensitivity is computed with respect to ω using (23) for the two cycles and compared to the finite-difference sensitivity (see Figure 3d). The adjoint sensitivities of both branches are in excellent agreement (difference $< 1 \times 10^{-6}$) with finite-difference analysis.

B. Optimization Results

Two forms of the forced Duffing oscillator are studied to test the optimization methodology. The first one corresponds to a strictly cubic hardening spring. The difficulties encountered in the optimization search are described and the tradeoff curve is computed for the two-objective problem. In the second application, a spring with combined softening and hardening is analyzed to demonstrate the robustness of the optimization search to softening nonlinearities (while retaining bounded solutions).

1. Cubic Hardening Nonlinearity

The optimization problem (1) is solved for the Duffing oscillator using parameters (Table 2) analyzed previously by the authors: a linear dynamic system[7] with an additional cubic nonlinear term (with $\beta = 0.3$). The cyclic form of the Duffing equation (25) is implemented in the study with $a = 1$. The design variables correspond to the actuation frequency, ω, and the instantaneous force at equally spaced locations over the cycle, f_i. The design variables are free to change within an upper and lower bounds corresponding to:

$$\omega_l \leq \omega \leq \omega_u, \tag{26a}$$

$$-f_{\max} \leq f_i \leq f_{\max}, \tag{26b}$$

where the upper, ω_u, and lower, ω_l, values of ω are set proportional to the system natural frequency, ω_n, and $f_{\max}$ is set based on the maximum permissible force available to the system.

The gradient-based optimization search is implemented using *fmincon* in Matlab, which is based on the sequential quadratic programming algorithm (SQP). The sensitivities of the objective and constraints are
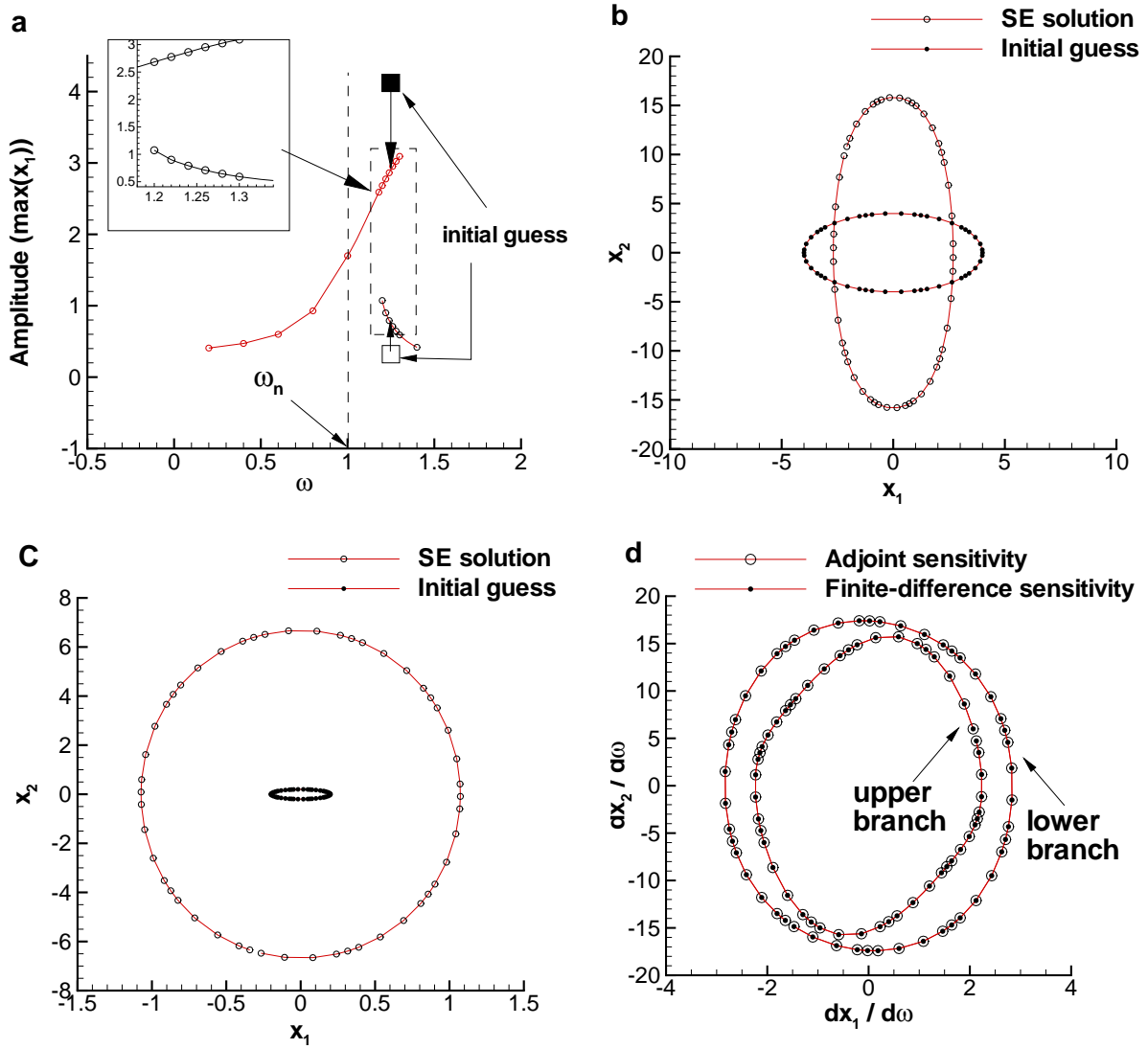
American Institute of Aeronautics and Astronautics

Figure 3. Solution of the hardening Duffing equation: a) response amplitude versus frequency, the x_1 amplitude of two different initial guesses are denoted by the two squares; **b)** response orbit at $\omega = 1.2$ and initial guess close to upper branch $(\max|x_1| \geq 4)$; **c)** response orbit at $\omega = 1.2$ and initial guess close to lower branch $(\max|x_1| \leq 0.2)$; **d)** comparison of response sensitivities at $\omega = 1.2$ computed using adjoint and finite-difference methods for both lower and upper branches.

Table 2. Fixed parameters of optimization problem for the cubic hardening Duffing equation.

ω_n	ω_l	ω_u	ζ	m	n_d	p	N_{el}	β	Objective tolerance	Constraint Tolerance
31.57	$\frac{2}{3}\omega_n$	$4\omega_n$	0.019	0.01	31	5	30	0.3	1×10^{-6}	1×10^{-6}

computed using the adjoint method. The optimization problem is solved for the actuation force history and period yielding the minimum work per cycle for a target displacement amplitude (1b). The tradeoff curve is constructed by solving the optimization problem for a series of target amplitudes.

Convergence of the optimization search hinges on the feasibility of enforcing the constraint on the target amplitude. In the previous section, we noted existence of multiple solutions (Figure 3) in the response near the resonant frequency of the linear system, and the subsequent dependence of the response on the initial guess in Newton's method. The optimization search tends to favor this complicated region in the design space. Therefore, to enable a successful optimization search, the later initial guess needs to be in coherence with the desired response. The formulation of the optimization problem as minimization of the work, while enforcing an upper constraint on the displacement amplitude, makes this choice rather simple by selecting the displacement initial guess close to the target displacement. This enables rapid convergence to the optimal design. A poor initial guess may lead the optimization search to a solution branch far from the desired one, resulting in an infeasible search.

The tradeoff curve of optimal work-and-amplitude is computed assuming different levels of permissible control force, $|f_{\max}|$. For example, the tradeoff curve for $|f_{\max}| = 1$ is constructed by solving the optimization problem five times, for each a different value of the target amplitude Γ_T: $\{0.5, 1.0, 1.5, 2.0, 2.5\}$. The lower and upper bounds of Γ_T may be selected based on the user preferences and system limitations. For each optimization search, the initial estimate of the control force is set to $|f_{\max}| \sin(0.9\omega_n t)$. The above procedure is repeated to generate a different tradeoff curve for a specific permissible control force $|f_{\max}|$.

The search for an optimal actuation is guided by the sensitivities of the objectives and constraints to the design variables. The sensitivities of the objective and amplitude with respect to the optimal control force are reported in Figure 4 for $\Gamma_T = 1$ and $|f_{\max}| = 1$. The figure indicates that the sensitivity of the objective (work per cycle) to a change in the instantaneous control force is larger than the sensitivity of the amplitude. However, the sensitivity of the objective and amplitude to change in ω is even larger: $\partial W/\partial \omega = -20.3$ and $\partial(\max|x_{ca}|)/\partial \omega = 6.6$. The large difference in the sensitivity magnitude between the design variables ω and f_i results in faster convergence of the former to the optimal design.
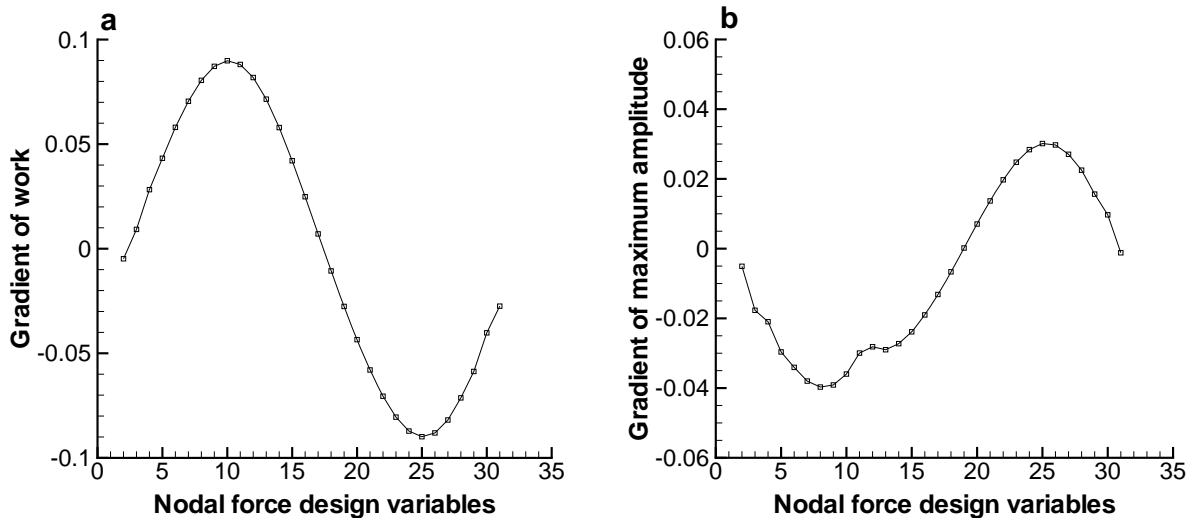

Figure 4. Cubic hardening Duffing equation: Gradients of the objective and maximum amplitude with respect to actuation design variables at a target amplitude of $\Gamma_T = 1$ and $|f_{\max}| = 1$ of the optimal design: a) objective; b) maximum amplitude.

The optimization results are reported in Table 3 and Figures 5a,b. Each curve in Figure 5a refers to a tradeoff curve of maximum amplitude and minimum work for a permissible $|f_{\max}|$. Data for the tradeoff curves are arranged column wise in Table 3. The tradeoff curve is indicated to have a quadratic relationship between $W_{\min}$ and Γ_T, which is similar to the analytical relationship between work and amplitude for linear systems with harmonic actuation [24, page 120]. This relationship is maintained as $|f_{\max}|$ is increased, where a more relaxed constraint on the control force enabled a decrease in the work necessary to achieve the same

American Institute of Aeronautics and Astronautics

target amplitude. As the control force is set to its lower limit, $|f_{\max}| = 1$, the optimization search is unable to enforce the constraint $\Gamma_T = 2.5$. To analyze the source of infeasibility, the frequency response of the optimal actuation at $\Gamma_T = 2.0$ and $|f_{\max}| = 1$ is reported in Figure 6 for both the linear and nonlinear systems. The peak of the frequency response diagram, $\max\left(\max|x_{ca}|\right)$ of the nonlinear system is slightly higher than 2.0 but less than 2.5 (=3.3 for the linear system). Consequently, the optimization search is unable provide a design due to the infeasibility of enforcing the amplitude constraint $\Gamma_T = 2.5$.

Optimal values of the forcing frequency corresponding to the tradeoff curves are shown in Figure 5b as a function of target amplitude. The optimal frequency, ω_o, is indicated to increase as the demand for larger amplitude is increased. This is similar to what is shown in Figure 3a, where the response amplitude increases for an increasing ω. However, at $|f_{\max}| = 6$, the optimal frequencies remained constant for $\Gamma_T = \{0.5, 1.0\}$. This occurs because at this large force, the initial response is significantly larger than the target one. Consequently, it is not required to increase ω to enforce the amplitude constraint. On the contrary, the frequency is allowed the opportunity to decrease in value to decrease the work objective until the lower limit of ω is reached (a more relaxed lower limit on ω may decrease ω_o even further for $\Gamma_T = 0.5$ and $\Gamma_T = 1.0$). Subsequent optimization iterations only refined the shape of the control force to further decrease the value of work while enforcing the amplitude constraint.

The shape of the optimal actuation at $|f_{\max}| = 6$ (see Figure 7a) strove to vary in an abrupt manner, with an extra cycle in the actuation trying to emerge. Orbits of the displacement and velocity responses for the optimal actuation are reported in Figure 7b,c, where the amplitude of the displacement is observed to satisfy the constraint, $\Gamma_T = 1.0$. When the constraint on the force is reduced ($|f_{\max}| = 1$), the abrupt behavior of the actuation becomes more apparent, see Figure 8a. Here, the optimization search compensates for the lack of available force $|f_{\max}|$ by a sudden change of the actuation.

In the absence of optimization, a designer may choose to actuate the system using a trivial harmonic force and vary the amplitude or frequency of actuation to find the best performance. Consider first varying the amplitude of $|f_{\max}|\sin\omega_n t$ (Table 4 and Figure 5c). The sinusoidal actuation is chosen at $\omega = \omega_n$ due to the anticipated large response at this frequency. A direct comparison to the results in Table 3 can be accomplished by solving for an $|f_{\max}|$, using a one-dimensional optimization search, that yields an amplitude, $\max(|x_{ca}|)$ equal to the target one, Γ_T. The value of expended work (not necessarily the minimum work) corresponding to the $\max(|x_{ca}|)$ is reported on the left ordinate axis. For small amplitude ($\Gamma_T = 0.5$), the benefits of optimization may not be clear, since the computed $|f_{\max}| = 0.34$ is much less than any of the enforced limits on the instantaneous force. For larger target amplitudes ($\Gamma_T \geq 1.0$) the amplitude of harmonic actuation necessary to achieve Γ_T increases substantially (see right ordinate axis in Figure 5c). In contrast, the optimal actuation does not need actuation forces nearly as large as the harmonic $|f_{\max}|$. Consider for example the second column in Table 4. To achieve the same target (=1.0), the amplitude of the harmonic actuation is two times the optimal one (first column in Table 3 with $|f_{\max}| = 1$). The optimal actuation for this case is reported in Figure 8a, and is seen to vary in a snap-type manner. This indicates that the optimal actuation trades force amplitude for a smaller and sharper variation in the control force to achieve the design requirements.

However, this exchange of smoothness and force does not occur at the expense of the work objective. The improvement in the work objective may be observed by comparing force amplitudes of harmonic actuation $|f_{\max}| = 7.25$ (third column in Table 4) with the optimal one $|f_{\max}| = 6.0$. Here we observe for the same maximum amplitude ($\Gamma_T = 1.5$) a 2.2% decrease in the work from the harmonic actuation, even with a 17% decrease in the optimal force amplitude. The comparison to other columns in Table 3 is not trivial, since the constraint on the force is much less than $|f_{\max}| = 7.25$.

Alternatively, the designer may vary the actuation frequency, while holding the force amplitude constant. The frequency corresponding to the optimal displacement amplitude is computed in a similar manner to selection of the force amplitude (see Table 5 and Figure 5d). To enable comparison with the tradeoff set, the force amplitude is fixed at $|f_{\max}| = 4$. The left and right ordinate axes of the figure display the respective work and frequency (not necessarily optimal) corresponding to $\max|x_{ca}|$. Although the same trend of variation in W as a function of $\max|x_{ca}|$ is observed, there is an increase in work ranging from 2-135% in comparison to the optimal designs. Furthermore, when the required power ($P = W/T$) is compared, the increase in power is in the range of 3 - 380%.

The variation of ω as a function of $\max|x_{ca}|$ (solid line) indicate a monotonic increase in amplitude. This is similar to the upper branch in Figure 6. However, for $\max|x_{ca}| = 0.5$, there are two possible frequencies at which $\max|x_{ca}| = 0.5$ may be attained. One in the lower branch -near the multiple solution region- and
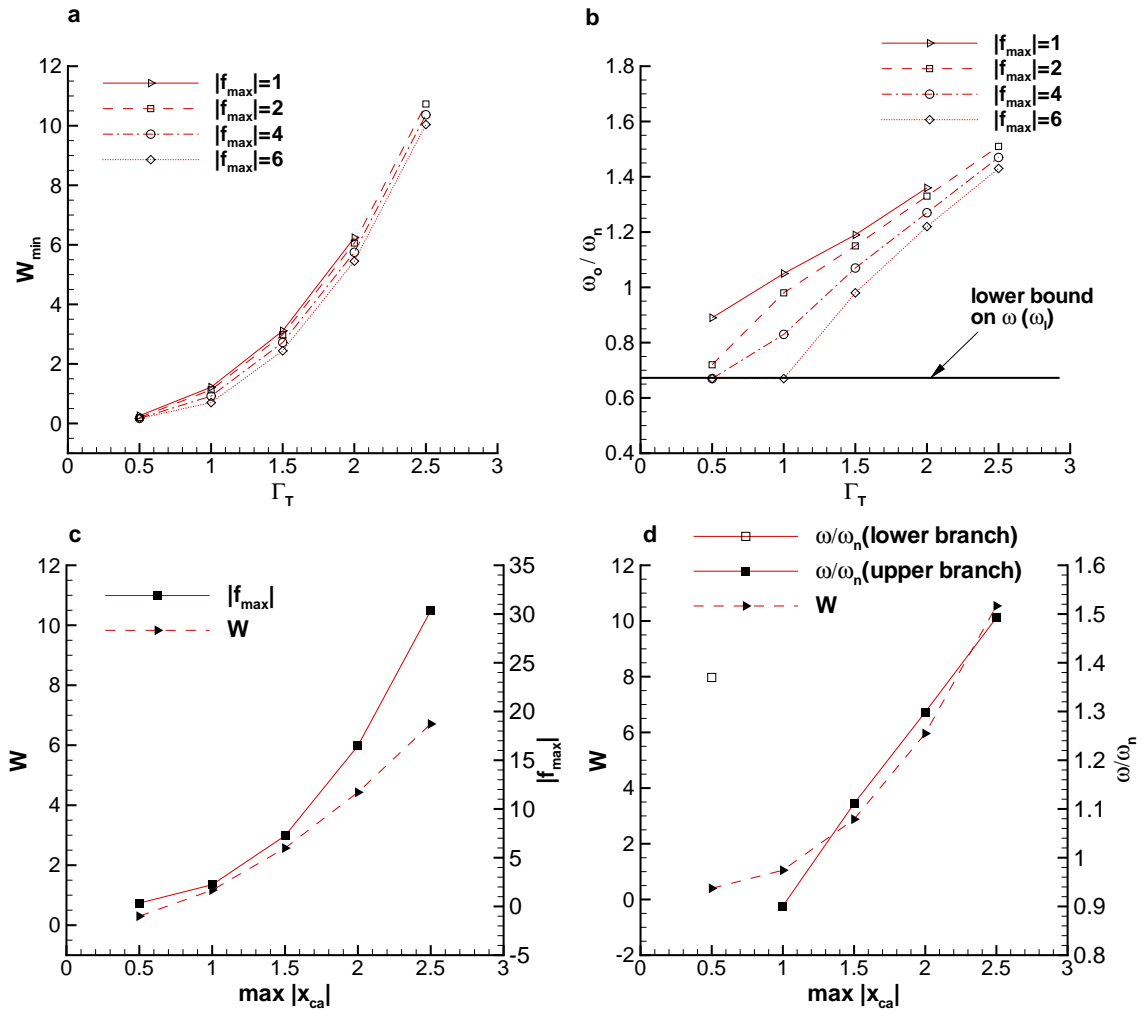
American Institute of Aeronautics and Astronautics

Figure 5. Optimization results of cubic hardening Duffing problem. The Pareto front is computed for different side constraints $|f_{\max}|$ on the force design variables: a) Pareto front, see Table 3; b) optimal periods of actuation corresponding to the Pareto front; c) work and maximum force amplitude values corresponding to a maximum displacement amplitude equal to the target one. The force variation conforms to a sinusoidal actuation at $\omega = \omega_n$ (see Table 4); d) work and period values corresponding to a maximum displacement amplitude equal to the target one. The force variation conforms to a sinusoidal actuation at $f_{\max} = 4$ (see Table 5).
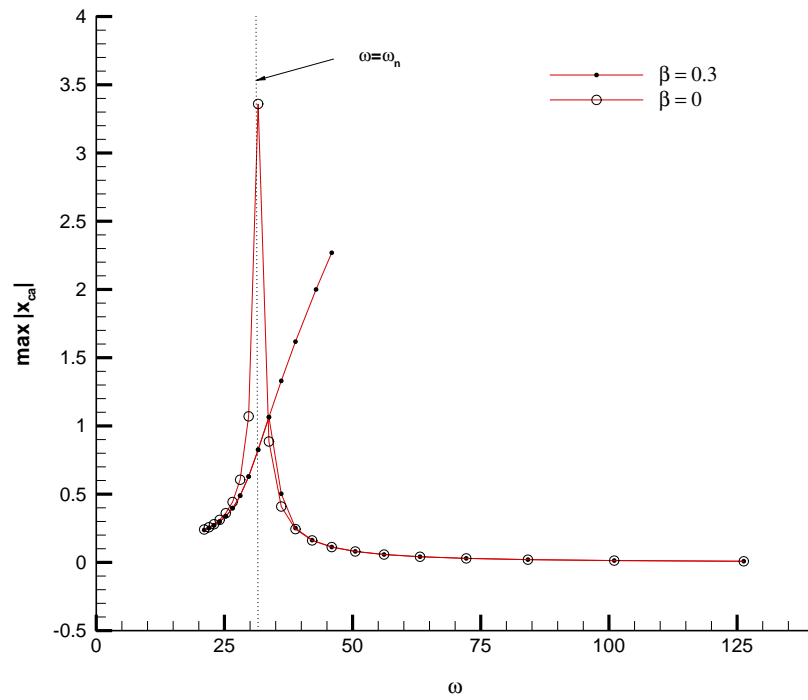
American Institute of Aeronautics and Astronautics

Figure 6. Frequency response of the cubic hardening Duffing system using the optimal actuation force for $\Gamma_T = 2$ and $f_{\max} = 1$.

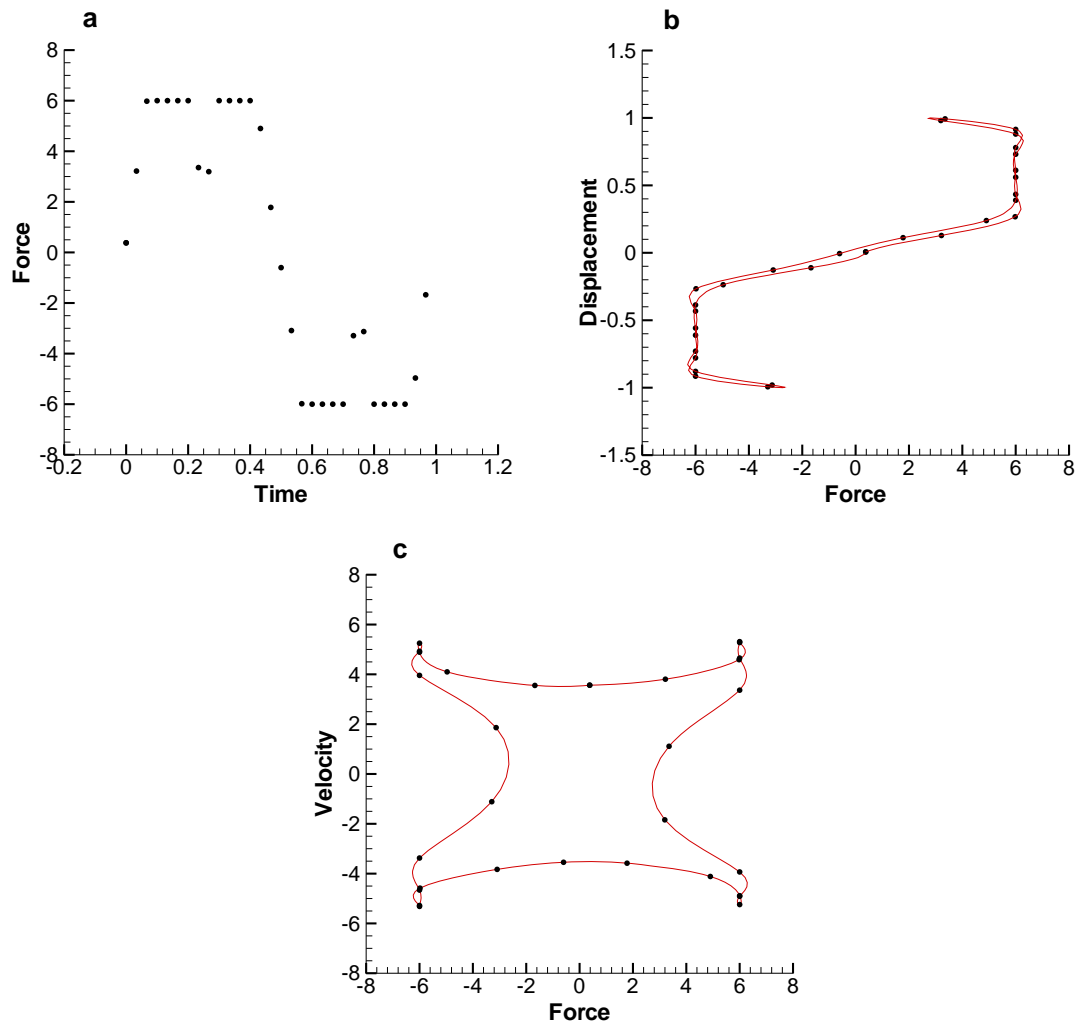American Institute of Aeronautics and Astronautics

Figure 7. Response of the cubic hardening Duffing equation for $\Gamma_T = 1$ and $f_{\max} = 6.0$ a) optimal actuation; b) orbit of optimal actuation and displacement response; and c) orbit of optimal actuation and velocity response.

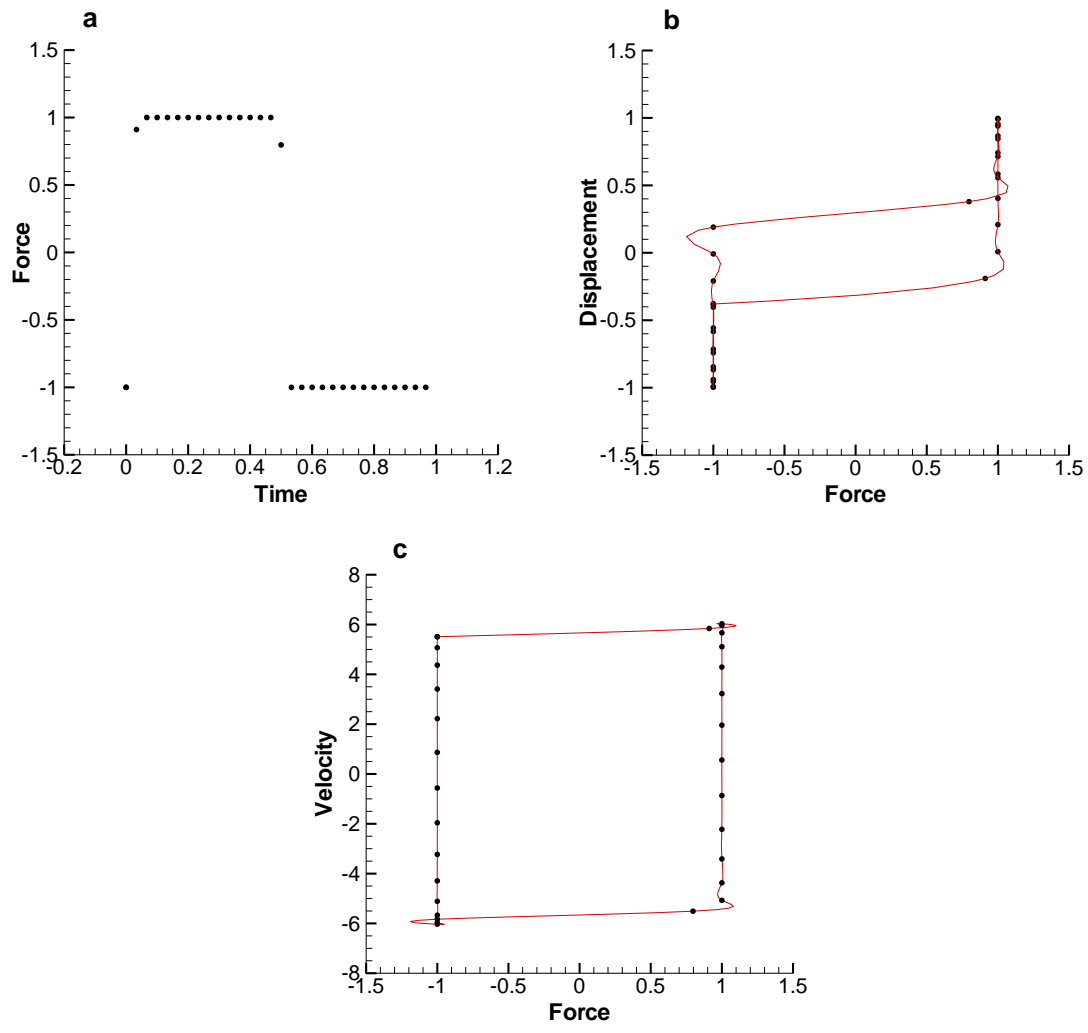American Institute of Aeronautics and Astronautics

Figure 8. Response of the Duffing equation for $\Gamma_T = 1$ and $f_{\max} = 1.0$ a) optimal actuation; b) orbit of optimal actuation and displacement response; and c) orbit of optimal actuation and velocity response.

American Institute of Aeronautics and Astronautics

the other in the upper branch of the frequency response diagram. The disjoint value indicated in the figure correspond to the former. In contrast the optimal frequency favored the upper branch at $\omega_o/\omega_n = 0.67$ in order to minimize the work.

Table 3. Pareto fronts optimal sets for a $\beta = 0.3$ and initial estimate of the control force corresponding to $|f_{\mathbf{max}}|\sin(0.9\omega_n t)$. Each Pareto set corresponds to an $|f_{\mathbf{max}}|$ side constraint on the control force design variables.

$|f_{\max}|$	1		2		4		6	
Γ_T	$W_{\min}$	ω_o/ω_n	$W_{\min}$	ω_o/ω_n	$W_{\min}$	ω_o/ω_n	$W_{\min}$	ω_o/ω_n
0.50	0.26	0.89	0.20	0.72	0.17	0.67	0.17	0.67
1.00	1.22	1.05	1.13	0.98	0.92	0.83	0.70	0.67
1.50	3.11	1.19	2.98	1.15	2.72	1.07	2.44	0.98
2.00	6.24	1.36	6.06	1.33	5.75	1.27	5.45	1.22
2.50	NF§	NF§	10.73	1.51	10.37	1.47	10.04	1.43

§ Not feasible

Table 4. Displacement amplitude ($\max(|x_{ca}|)$) and expended work W for $|f_{\max}|\sin\omega_n t$. The amplitude of the control force $|f_{\max}|$ is computed to yield a displacement amplitude equal to the target one in the Pareto front, see Table 3.

$\max(|x_{ca}|)$	0.5	1.0	1.5	2.0	2.5
W	0.30	1.17	2.57	4.43	6.71
$|f_{\max}|$	0.34	2.23	7.25	16.48	30.35

Table 5. Displacement amplitude ($\max(|x_{ca}|)$) and expended work W for $|f_{\max}|\sin\omega t$ with $|f_{\max}| = 4$. The frequency of the control force is computed to yield a displacement amplitude equal to the target one in the Pareto front, see Table 3.

$\max(|x_{ca}|)$	0.5	1.0	1.5	2.0	2.5
W	0.40	1.04	2.88	5.96	10.54
ω/ω_n	1.37	0.91	1.11	1.30	1.49

2. Softening-and-Hardening Nonlinearity

A softening Duffing system results when the coefficient of nonlinearity is negative, i.e., the spring stiffness decrease as deflection increases. The softening is relevant to many physical phenomena such as rolling motion of a ship[25] or longitudinal vibrations of piezoceramic rods.[26] The hardening system is characterized by a jump-down frequency, where the amplitude jumps down for an increasing frequency sweep. When the nonlinearity is of softening type, a jump-up frequency occurs. Recently, Berennan et al.[27] and Malatkar and Nayfeh [28] calculated these frequencies for either a softening or hardening cubic nonlinearities. In this section, the optimal actuation of a combined softening-and-hardening Duffing system is analyzed. The cubic coefficient is selected to provide softening, whereas the pentic coefficient provides hardening. In this manner, the system near resonance softens and encourages response until the restraining nonlinearity dominates. Parameters of the system are listed in Table 7. The jump-up and jump-down behavior is observed by computing the frequency response of the system for a harmonic force of unit amplitude. The response is reported in Figure 9. The response is indicated to possess a double discontinuity due to the simultaneous hardening and softening effects.

The optimization problem is applied to this system to test the robustness of the gradient-based search method. Results of the optimization search are listed in Table 7. The initial estimate of the design force is $\sin(\omega_i t)$. The initial design is denoted with the subscript i. Two optimization problems are solved for target amplitudes $\Gamma_T = 0.5$ and $\Gamma_T = 1.0$. The optimal actuation for each target are indicated in Figure 10.

For $\Gamma_T = 0.5$ the response to the initial harmonic design ($\omega_i = 0.91\omega_n$) is larger than the demanded one (see Figure 9). This allows the optimization search the opportunity to decrease the work by around 80%, until the amplitude constraint becomes active. The optimal design enabled this improvement by first adjusting the actuation frequency and then the instantaneous force, see Figure 10a. However, for $\Gamma_T = 1.0$, the initial design response is close to the target one. There, the decrease in work objective competes with the enforcement of the amplitude constraint. The optimal actuation force compensates for this by varying the force in a snap-type manner. See Figure 10b. Comparison of the minimum work with the initial work indicates a 13% decrease for almost the same response amplitude.

Furthermore, the optimal design at $\Gamma_T = 0.5$ can not be easily compared to the harmonic one, since the frequency response is discontinuous near $\max|x_{ca}| = 0.5$; see Figure 9. In this case, the optimization search penetrates a region in the design space inaccessible by the trivial design by varying the instantaneous actuation force. Without the optimization search and the ability to tailor the actuation force, this response may only be possible by using larger force amplitude than the resources permit.
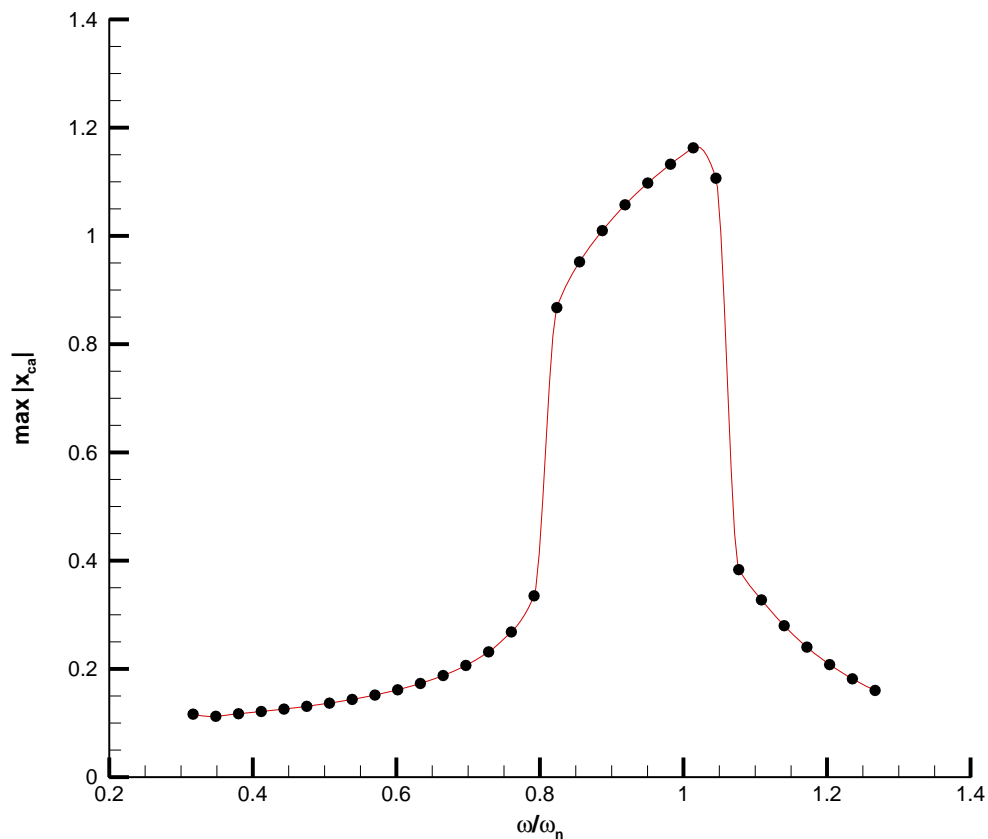

Figure 9. Frequency response diagram of softening-and-hardening Duffing system using harmonic actuation, $\sin\omega t$.

American Institute of Aeronautics and Astronautics

Table 6. Fixed parameters of optimization problem for the softening-and-hardening Duffing system.

$|f_{\max}|$	ω_n	ω_l	ω_u	ζ	m	n_d	p	N_{el}	β	γ	Objective tolerance	Constraint Tolerance
1	31.57	$\frac{2}{3}\omega_n$	$4\omega_n$	0.019	0.01	31	5	30	-1	1	1×10^{-6}	1×10^{-6}

Table 7. Optimization results of softening-and-hardening Duffing system for $|f_{\max}| = 1$.

Γ_T	$W_{\min}$	ω_o/ω_n	W_i	ω_i/ω_n	$\max|x_{ca}|_{,i}$
0.5	0.23	0.79	1.14	0.91	1.04
1.0	0.99	0.86	1.14	0.91	1.04

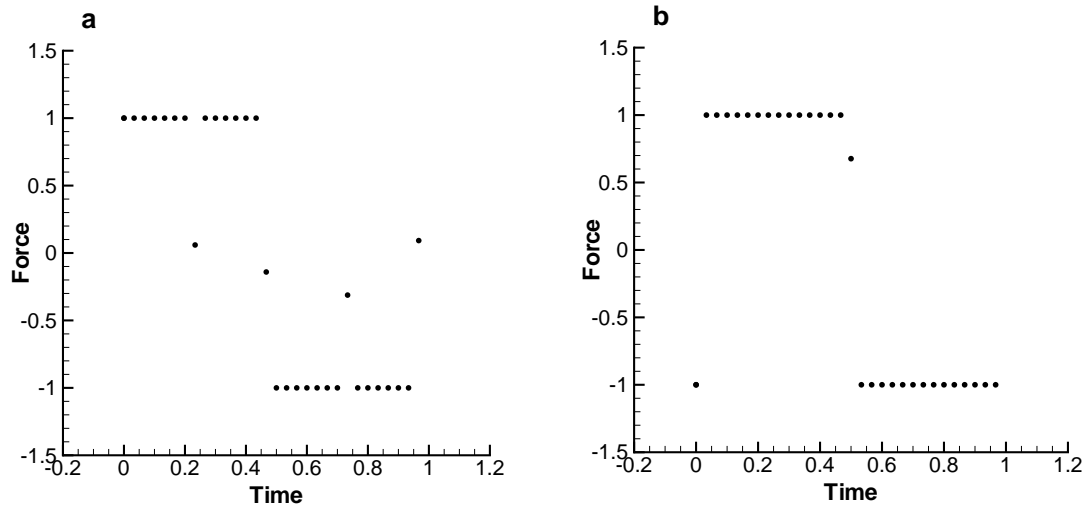**Figure 10. Optimal actuation force of the softening-and-hardening Duffing system at $|f_{\max}| = 1$: a) $\Gamma_T = 0.5$; b) $\Gamma_T = 1.0$.**

American Institute of Aeronautics and Astronautics

VI.   Conclusions

In this paper, a formulation is developed to compute the optimal actuation of nonlinear, resonant dynamic systems for the dual objectives of minimized actuation work and maximized amplitude of the time-periodic response. The constraint method is used to compute the tradeoff curve of both objectives by minimizing the actuation work for a set of constraints on the response amplitude. The nonlinear dynamic response of the periodic actuation is computed over one cycle using the monolithic-time spectral element method. The actuation force is constructed using the values of numerous design variables at equally spaced nodes in a cycle. Cubic splines are used to interpolate the force between any two variables. The adjoint sensitivity method is developed for the monolithic-time method to enable efficient gradient-based optimization search considering the large number of design variables.

The optimization methodology is applied to Duffing systems with cubic nonlinear hardening and cubic/pentic nonlinear hardening and softening. In the softening case, an additional pentic hardening spring is considered. The strict hardening application demonstrates the superiority of the optimization formulation in resolving dependence of nonlinear response on initial conditions, where the initial conditions are selected close to the specified constraint on the response amplitude. The tradeoff curves of minimum work and maximum amplitude are computed for different levels of maximum available force. The optimal designs are compared to harmonic actuation yielding the same maximum amplitude. For equal force amplitudes, the work of harmonic actuation is found to be 2-135% larger than the optimal one. However, when the demand on the response is large, the harmonic actuation can only enforce the constraint using a large-force amplitude. The optimal actuation compensates for the limited available force by varying the force abruptly in time. In some cases, to attain the same response, a 20% increase in the harmonic force is needed over the optimal one, although the latter resulted in a 2.2% work savings. The application of optimization formulation to Duffing system with softening and hardening verified robustness of the search method and showed similar improvements in the performance measures. Additionally, the optimal design is found to yield designs in regions deemed discontinuous using harmonic actuation.

References

[1]W. Shyy, M. Berg, and D. Ljungqvist. Flapping and flexible wings for biological and micro air vehicles. *Progress in Aerospace Sciences*, 35(5):455 – 505, 1999.

[2]M. Blair, G.H. Parker, P.S. Beran, and R.D. Snyder. A computational design framework for flapping Micro Air Vehicles. AIAA Paper 2007-763.

[3]R.D. Snyder, P.S. Beran, G.H. Parker, and M. Blair. A design optimization strategy for Micro Air Vehicles. AIAA Paper 2007-1853.

[4]K. Palaniappan, P.S Beran, and A. Jameson. Optimal control of LCOs in aero-structural systems. AIAA-2006-1621.

[5]Caspar T. Bolsman, Johannes F.L. Goosen, and Fred Van Keulen. Insect-inspired wing actuation structures based on ring-type resonators. volume 6928, 2008.

[6]M.H. Kurdi and P.S Beran. Optimization of dynamic response using temporal spectral element method. AIAA-2008-0903.

[7]M.H. Kurdi and P.S Beran. Optimization of dynamic response using a monolithic-time formulation. *Structural Design and Multidisiplinary Optimization*, submitted 2008.

[8]D.L. Raney and E.C Slominski. Mechanization and control concepts for biologically inspired mirco air vehicles. *Journal of Aircraft*, 41(6):1257–1265, 2004.

[9]V.B. Venkayya, N.S. Khot, V.A. Tischler, and Taylor R.F. Design of optimum structures for dynamic loads. In *the 3rd Conference on Matrix Methods of Structural Mechanics*, pages 619–658, Flight Dynamics Laboratory, Wright Patterson Air Force Base, Ohio, October 1971.

[10]R.T. Haftka. Parametric constraints with application to optimization for flutter using a continuous flutter constraint. *AIAA Journal*, 13(4):471–475, 1975.

[11]C. C. Hsieh and J. S. Arora. Design sensitivity analysis and optimization of dynamic response. *Applied Mathematics and Optimization*, 43(2):195 – 219, 1984.

[12]R.V. Grandhi, R.T. Haftka, and Layne T. Watson. Design oriented identification of critical times in transient response. AIAA Paper 1984-0899.

[13]R.V. Grandhi, R.T. Haftka, and L.T. Watson. Efficient identification of critical stresses in structures subject to dynamic loads. *Computers and Structures*, 22(3):373 – 86, 1986.

[14]A.T. Patera. A spectral element method for fluid dynamics; laminar flow in a channel expansion. *Journal of Computational Physics*, 54:468–488, 1984.

[15]R.H. Rand. Lecture notes on nonlinear vibrations. http://www.tam.cornell.edu/randdoc/, 2005.

[16] J.M.T. Thompson. An introduction to nonlinear dynamics. *Applied Math Modeling*, 8:157–168, 1984.

[17] M.H. Kurdi, T.L. Schmitz, R.T. Haftka, and B.P. Mann. Milling optimization of removal rate and part accuracy - part 1: Parameter selection. *International Journal of Materials Product and Technology*, accepted 2007.

[18] G.E. Karniadakis and S.J. Sherwin. *Spectral/hp element methods for CFD*. Oxford University Press, 1999.

[19] C. Pozrikidis. *Introduction to finite and spectral element methods using Matlab*. Chapman and Hall/CRC, 2005.

[20] D.S. Burnett. *Finite element analysis; from concepts to applications*. Addison-Wesley, 1988.

[21] M.H. Kurdi and P.S. Beran. Spectral element method in time for rapidly actuated systems. *Journal of Computational Physics*, 227(3):1809–1835, 2008.

[22] S. Timoshenko and D.H. Young. *Vibration Problems in Engineering*. D. Van Nostrad, Inc., New York, third edition, 1955.

[23] B.H.K. Lee, L. Gong, and Y.S. Wong. Analysis and computation of nonlinear dynamic response of a two-degree-of-freedom system and its application in aeroelasticity. *Journal of fluid and structures*, 11(3):225 – 246, 1997.

[24] R.F. Jr Steidel. *An introduction to mechanical vibrations*. John Wiley and Sons, 1989.

[25] A.H. Nayfeh and N.E. Sanchez. Bifurcation in a forced softening duffing oscillator. *International Journal of Nonlinear Mechanics*, 24(6):483–497, 1989.

[26] U. von Wagner. Non-linear longitudinal vibrations of non-slender piezoceramic rods. *International Journal of Non-Linear Mechanics*, 39(4):673 – 88, 2004.

[27] M.J. Brennan, I. Kovacic, A. Carella, and T.P. Waters. On the jump-up and jump-down frequencies of the duffing oscillator. *Journal of Sound and Vibration*, in press 2008.

[28] P. Malatkar and A.H. Nayfeh. Calculation of the jump frequencies on the response of a s.d.o.f. nonlinear system. *Journal of Sound and Vibration*, 254(5):1005–1011, 2002.

A. Convergence of Newton Method: Duffing

The convergence properties of the nonlinear solution is reported in Figure 11 for the Duffing problem with strict cubic hardening. The nonlinear solution is computed using (18). Iterations are started using a harmonic initial guess with an amplitude $\epsilon = 1 \times 10^{-6}$. The residual (15) is reported as a function of iteration number, where the jacobian is evaluated for the first 20 iterations and frozen for larger iterations. Solution of the Duffing system is computed for a sinusoidal actuation force using a forcing frequency equal to the natural frequency of the linear system ($\omega_n = 31.57$) and far from the natural frequency ($=0.7\omega_n$). The standard quadratic convergence rate of the Newton method is attained for $0.7\omega_n$, however the convergence rate deteriorates for $\omega = \omega_n$.
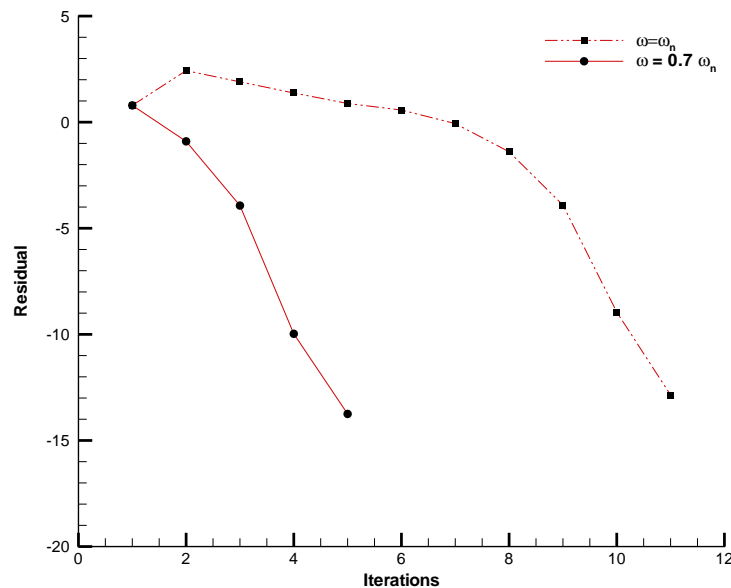

Figure 11. Convergence of the nonlinear solution for the hardening Duffing system $\beta = 0.3$ using a harmonic actuation $\sin \omega t$. Convergence rate deteriorates near the natural frequency.

American Institute of Aeronautics and Astronautics